SF2A 2024
M. Béthermin, K. Baillié, N. Lagarde, J. Malzac, R.-M. Ouazzani, J. Richard, O. Venot, A. Siebert (eds)

THERMAL TIDES ON ROCKY PLANETS THROUGH A NOVEL FULLY ANALYTICAL SOLUTION

P. Auclair-Desrotour[1], M. Farhat[1], G. Boue[1], R. Deitrick[2] and J. Laskar[1]

Abstract. Thermal tides are atmospheric tides caused by variations in day-night insolation, similar to gravitational tides but with key differences. While both result in delayed mass redistribution, energy dissipation, and angular momentum exchanges between the planet and its host star, thermal tides can drive a planet's dynamics away from the rotational equilibrium states predicted by classical tidal theory. In this work, we present a novel closed-form solution for the thermotidal response of rocky planets. This general solution is derived from first principles, assuming either dry or moist adiabatic temperature profiles for the planet's atmosphere, and can be readily applied to study the long-term evolution of exoplanets in the habitable zones of their host stars. Despite relying on a small number of parameters, the model successfully captures the key features of the thermotidal torque predicted by General Circulation Models (GCMs). It also accurately predicts Earth's current semidiurnal thermotidal response and provides new insights into the evolution of the length of day during the Precambrian era.

Keywords: Earth – Planets and satellites: terrestrial planets – Planets and satellites: atmospheres – Planet-star interactions – Planets and satellites: dynamical evolution and stability

1 Introduction

It has long been recognised that Solar irradiation induces atmospheric thermal tides, similar to gravitational forces. These tides arise from the difference in thermal forcing between the day and night sides of the planet, with the dayside heated by the star and the nightside cooling radiatively (e.g. Chapman & Lindzen 1970). This leads to a denser atmosphere on the nightside, causing global redistribution of mass, akin to oceanic and solid tides. As early as the late 19th century, Lord Kelvin quantified the thermotidal torque, arising from this mass redistribution, on Earth's spin axis using barometric measurements (Kelvin 1882), finding it to be approximately 7% of the torque from gravitational tides in the Earth's oceans and solid interior (e.g. Lambeck 1977), despite the tiny planet's mass fraction constituted by the atmosphere ($\sim 8.5 \times 10^{-5}$ %)*.

Earth's semidiurnal thermal tide is phase-advanced relative to the Sun, with surface pressure oscillations peaking around 09:45 LST (Local Solar Time) and 22:00 LST (Dai & Wang 1999; Schindelegger & Ray 2014; Auclair-Desrotour et al. 2017), unlike gravitational tides, which are always delayed. The resulting accelerative thermotidal torque increases Earth's spin over time. This effect is also seen on Venus, where it counteracts the torque from solid tides, leading to asynchronous rotation (Gold & Soter 1969; Ingersoll & Dobrovolskis 1978; Correia & Laskar 2001; Correia et al. 2003; Correia & Laskar 2003; Leconte et al. 2015). Thermal tides can similarly induce differential rotation on hot Jupiters (e.g. Arras & Socrates 2010; Auclair-Desrotour & Leconte 2018; Gu et al. 2019; Lee 2020) and determine the rotational states of near synchronous rocky exoplanets (e.g. Laskar & Correia 2004; Correia & Laskar 2010; Cunha et al. 2015; Leconte et al. 2015; Auclair-Desrotour et al. 2017, 2019).

While the thermotidal torque on present-day Earth contributes only minimally to the total torque, the atmosphere may have significantly influenced Earth's past rotational history. Like ocean tides, thermal forcing can excite planetary-scale compressibility waves known as Lamb waves (Lamb 1911; Bretherton 1969;

[1] IMCCE, Observatoire de Paris, Université PSL, CNRS, Sorbonne Université, 77 Avenue Denfert-Rochereau, Paris, 75014, France
[2] School of Earth and Ocean Sciences, University of Victoria, Victoria, British Columbia, Canada
*`https://nssdc.gsfc.nasa.gov/planetary/factsheet/earthfact.html`.

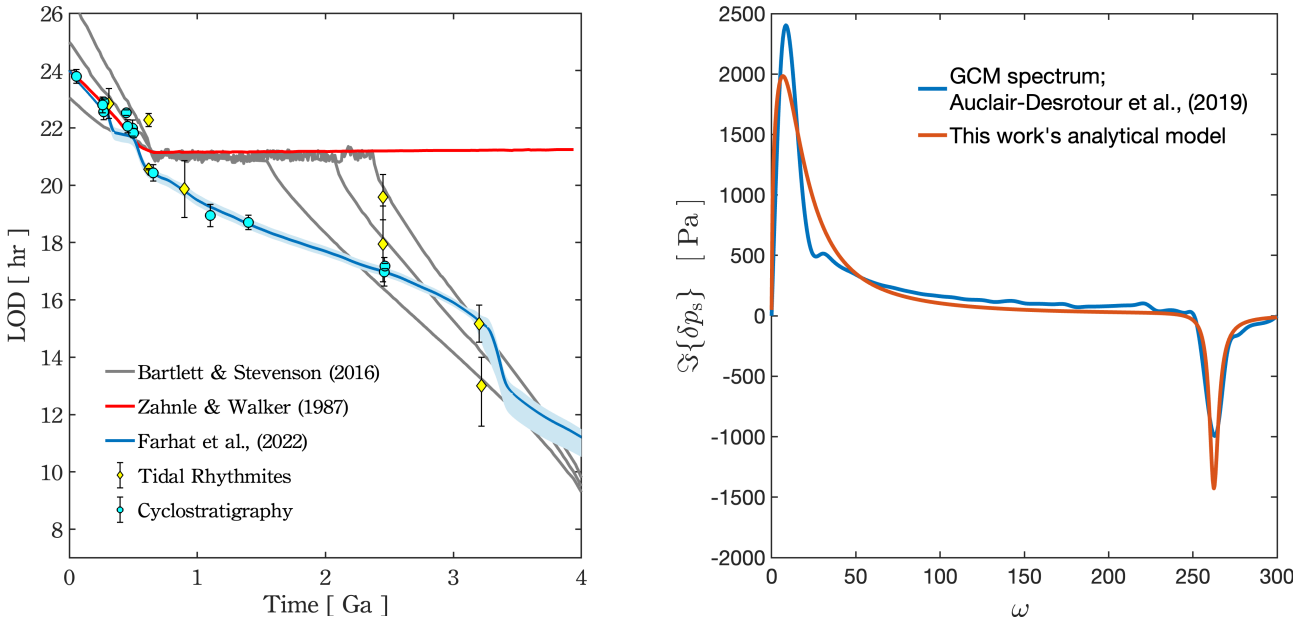

Fig. 1. Left: Modelled evolution of the Earth's LOD over geological timescales, shown for three different models: (i) Farhat et al. (2022), where the evolution is driven solely by oceanic and solid tidal dissipation; (ii) Zahnle & Walker (1987), where the resonance of the Lamb wave occurs at a LOD of ∼21 hr, imposing a rotational equilibrium on Earth; and (iii) Bartlett & Stevenson (2016), who propose equilibrium scenarios with the potential to escape tidal locking. **Right:** Imaginary part of the tidal surface pressure oscillations as a function of the normalised semidiurnal frequency $\omega = \sigma/(2n_\star)$ obtained (i) from GCM simulations by Auclair-Desrotour et al. (2019) (blue line), and (ii) by fitting the analytical model of F24 (Eq. (2.4)) to this numerical result (red line).

Lindzen & Blake 1972), analogous to the long-wavelength surface gravity modes in ocean tides. Resonance occurs when the eigenperiod of a Lamb wave matches the semidiurnal period. Given that Earth's current 12-hour semidiurnal period is close to resonance, Zahnle & Walker (1987) proposed that such a resonance occurred during the Precambrian era ($4587 - 538$ Myr ago), when the length of day (LOD) was around 21 hours. With gravitational tidal torque then about a quarter of today's, they suggested that Earth's LOD may have reached equilibrium and remained stable for hundreds of millions of years, as shown by Fig. 1 (left panel). Decades after this rotational equilibrium scenario was suggested for the Earth, Bartlett & Stevenson (2016) revisited the problem and tested the stability of the equilibrium to temperature changes on Earth. More recently, Mitchell & Kirscher (2023) and Wu et al. (2023) made use of the growing abundance of geological proxies on the Earth's rotational history to support the scenario originally proposed by Zahnle & Walker (1987).

In two recent papers, (Farhat et al. 2024; Laskar et al. 2024, hereafter F24 and L24), we explore the equilibrium hypothesis using an analytical approach. These studies build on Farhat et al. (2022), who reconstructed the Earth-Moon system's history based solely on oceanic and solid tidal dissipation. In F24, we present a closed-form solution for the tidal response of neutrally stratified atmospheres, dependent on tidal frequency and a few key physical parameters. This model shows strong agreement with General Circulation Models (GCM) simulations from previous work. Applied to Earth, our findings suggest that the resonant amplification of the thermotidal torque was insufficient to counter the torque arising from gravitational tides in the oceans, challenging the tidal locking hypothesis. The second paper, L24, complements F24 by reviewing recent research on the equilibrium problem and geological records. The following discussion focuses on key results from F24, with all figures taken from that work.

2 New general prescription for thermotidal atmospheric torque

We consider a star with mass $M_\star$ hosting a rocky planet of mass M, radius R, surface gravity g, and spin rate Ω. The planet's atmosphere, assumed to be thin, has a typical thickness given by the pressure scale height at the surface, $H_\mathrm{s} = R_\mathrm{s} T_\mathrm{s}/g$, where R_s is the specific gas constant ($R_\mathrm{s} = R_\mathrm{PG}/m_\mathrm{atm}$, with R_PG being the universal gas constant and m_atm the mean molecular weight), and T_s denotes the globally averaged surface temperature. For

a circular orbit of radius a and mean motion $n_\star$, within the planet's equatorial plane, the thermotidal torque reduces to the semidiurnal component,

$$\mathcal{T}_z = \sqrt{\frac{6\pi}{5}} \frac{M_\star}{M} \frac{R^6}{a^3} \Im \left\{ \delta p_{2,2} \left(\sigma \right) \right\}. \tag{2.1}$$

Here, $\sigma = 2\left(\Omega - n_\star\right)$ represents the semidiurnal tidal frequency, $\Im$ refers to the imaginary part of a complex number (with $\Re$ referring to the real part), and $\delta p_{2,2}$ is the degree-2, order-2 complex component in the spherical harmonic expansion of the tidal pressure oscillation, which captures the frequency-dependent atmospheric response. Additionally, we define the corresponding stellar flux component, $\delta F_{\star;2,2}$, the resonant frequency of the main forced Lamb wave, σ_L, and a constant pressure factor, δp_0,

$$\delta F_{\star;2,2} = \frac{\sqrt{30\pi}}{16} F_\star, \quad \sigma_\mathrm{L} = \frac{\sqrt{\Lambda_2 g H_\mathrm{s}}}{R}, \quad \delta p_0 = \frac{\kappa \alpha_\mathrm{A} \delta F_{\star;2,2}}{H_\mathrm{s} \sigma_\mathrm{L}}, \tag{2.2}$$

where $F_\star$ is the incident flux at the sub-stellar point, Λ_2 is the eigenvalue of the Hough function[†] that primarily overlaps with the thermal forcing distribution, $\kappa = R_\mathrm{s}/C_p$ (with C_p the heat capacity per unit mass), and α_A is the fraction of absorbed flux ($0 \leq \alpha_\mathrm{A} \leq 1$). For simplicity, we assume that Λ_2 is a constant with value $\Lambda_2 = 11.129$, which corresponds to Earth-like scenarios where $n_\star \ll \Omega$. The variations of Λ_2 near synchronisation and their potential implications on the atmospheric tidal response are thus neglected.

Finally, the atmosphere is assumed to be neutrally stratified, meaning that no Archimedean forces are present, and tidal waves are restored solely by horizontal compressibility. Although idealised, this atmospheric structure more realistically describes the convective troposphere of rocky planets than the classical isothermal assumption. Energy dissipation occurs through Newtonian cooling (i.e., linearised radiative cooling), characterised by the frequency σ_0. Under these conditions, Laplace's tidal equations can be solved analytically within linear theory (e.g. Lindzen & McKenzie 1967), yielding

$$\delta p_{2,2} = \delta p_0 \frac{G\left(X\right)}{\varepsilon \left[\left(\kappa + 1 \right) X^2 - 1 \right] + i X \left(X^2 - 1 \right)}, \tag{2.3}$$

where i denotes the imaginary unit, $X = \sigma/\sigma_\mathrm{L}$ is the normalised tidal frequency ($X = 1$ at resonance), $\varepsilon = \sigma_0/\sigma_\mathrm{L}$ is the damping coefficient, and the transfer function $G\left(X\right)$ accounts for soil diffusion effects in case of indirect radiative forcing in the infrared (with $G\left(X\right) = 1$ for direct absorption). The imaginary part, $\Im\left\{\delta p_{2,2}\right\}$, used in Eq. (2.1), is expressed as

$$\Im\left\{\delta p_{2,2}\right\} = \delta p_0 \frac{X\left(1 - X^2\right) \Re\left\{G\left(X\right)\right\} + \varepsilon \left[\left(\kappa + 1 \right) X^2 - 1 \right] \Im\left\{G\left(X\right)\right\}}{X^2 \left(1 - X^2\right)^2 + \varepsilon^2 \left[\left(1 + \kappa \right) X^2 - 1 \right]^2}, \tag{2.4}$$

and is plotted in Fig. 1 after fitting to Auclair-Desrotour et al. (2019)'s numerical results. For $G\left(X\right) = 1$ (direct absorption) and $X \ll 1$ (near-synchronised planets), Eq. (2.3) simplifies to

$$\delta p_{2,2} \approx -\frac{\delta p_0}{\varepsilon + i X}, \tag{2.5}$$

matching earlier analytical or GCM-based predictions for Venus-like planets (Ingersoll & Dobrovolskis 1978; Leconte et al. 2015; Auclair-Desrotour et al. 2019; Salazar & Wordsworth 2024).

3 Model predictions for Earth's past evolution

Observationally consistent estimate of present-day torque The analytical solution derived from Eqs. (2.1) and (2.4) allows for a broad exploration of the parameter space. When applied to Earth, it offers fresh insights into the equilibrium hypothesis. Notably, its prediction of the present-day thermal torque aligns well with estimates obtained from global barometric measurements (e.g. Schindelegger & Ray 2014).

[†]Hough functions are the functions used on the sphere to describe the spatial dependence of the tidal response (e.g. Wang et al. 2016).

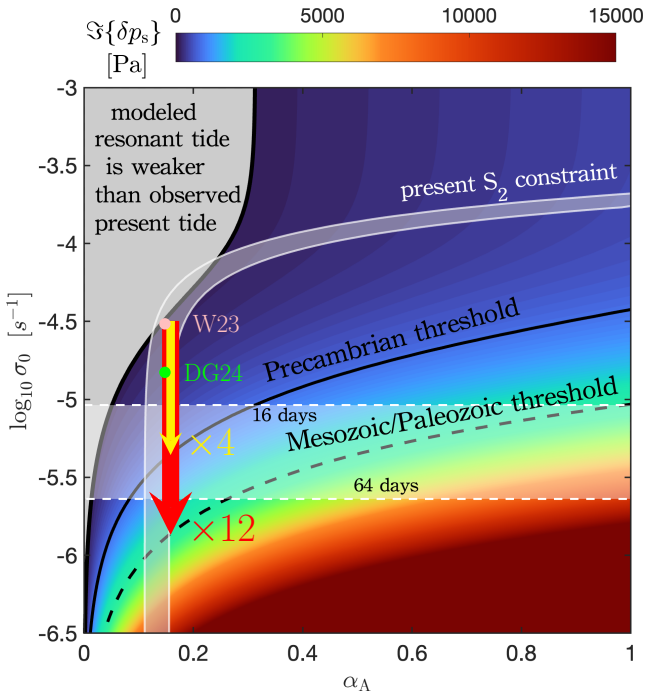

Fig. 2. Maximum reached by the imaginary part of the semidiurnal surface pressure component given by Eq. (2.4) as a function of the atmospheric opacity and radiative cooling frequency. The black solid and dashed lines define, from below, regions where the thermotidal response is sufficient to cancel the gravitational counterpart in the Precambrian ($4587-538$ Myr) and the late Paleozoic/early Mesozoic ($350-250$ Myr). The shaded areas indicate the contraints on α_A and σ_0 derived from observations and GCM simulations, along with the corresponding radiative timescales. The yellow and red arrows indicate the amplification factors needed to reach the Precambrian and Mesozoic/Paleozoic thresholds, respectively. The pink and green dots represent the GCM simulations of Wu et al. (2023), Fig. S4 (W23), and of Deitrick & Goldblatt (2024), Fig. 1 (DG24), respectively. Figure adapted from F24, Fig. 5.

Late resonance crossing Figure 2 illustrates the maximum value of the imaginary part of the semidiurnal surface pressure component, plotted against atmospheric opacity and radiative cooling frequency for direct forcing ($G(X) = 1$ in Eq. (2.4)). Observational and numerical constraints suggest that the minimum thermotidal torque required to balance gravitational torque during the Precambrian could only have been achieved with cooling timescales near the upper limits predicted by GCM simulations. The model in F24, however, suggests that resonance more likely occurred during the Mesozoic or the Paleozoic eras, when oceanic tidal dissipation was stronger (Zahnle & Walker 1987; Farhat et al. 2022). The thermotidal response at resonance appears insufficient to reach the Mesozoic/Paleozoic threshold shown in Fig. 2.

Limited resonant amplification It is worth noting that the solution provided by Eq. (2.4) likely overestimates the strength of the thermal tide at resonance, as non-linear dissipative processes are expected to damp tidal waves more effectively than the Newtonian cooling model used here. GCM simulations tend to confirm this, predicting resonant amplification factors of around 1.5 (Wu et al. 2023; Deitrick & Goldblatt 2024), whereas factors of approximately 4 or 12 would be required to reach the Precambrian or Mesozoic/Paleozoic thresholds, respectively.

Symmetry-breaking effect of soil diffusion The resonance of the Lamb wave is characterised by two peaks: one accelerative, potentially responsible for tidal locking, and one braking, which slows the planet's spin similarly to gravitational tides. In GCM simulations, the accelerative peak is significantly weaker than the braking one (Auclair-Desrotour et al. 2019; Wu et al. 2023; Deitrick & Goldblatt 2024), further arguing against the equilibrium hypothesis. This asymmetry can be captured in the analytical model by incorporating the effects of soil diffusion and indirect thermal forcing in the infrared by the ground, as shown in Fig. 1 (right panel).

4 Conclusions

By applying classical tidal theory to an atmosphere with neutral stratification and radiative cooling, we derived a new solution describing the frequency-dependent thermotidal torque exerted on a rocky planet's spin axis. This solution reflects key features previously identified in GCM simulations and has been validated against observational data. When combined with GCM results, the model's main predictions suggest that tidal locking likely never occurred on Earth. The derived expression for the thermotidal torque is particularly valuable for exoplanet studies investigating the tidal spin evolution of rocky planets with atmospheres.

This work has been supported by the French Agence Nationale de la Recherche (AstroMeso ANR-19-CE31-0002-01) and by the European Research Council (ERC) under the European Union's Horizon 2020 research and innovation program (Advanced Grand AstroGeo-885250). This work was granted access to the HPC resources of MesoPSL financed by the Region Île-de-France and the project Equip@Meso (reference ANR-10-EQPX-29-01) of the programme Investissements d'Avenir supervised by the Agence Nationale pour la Recherche.

References

Arras, P. & Socrates, A. 2010, The Astrophysical Journal, 714, 1

Auclair-Desrotour, P., Laskar, J., & Mathis, S. 2017, Astronomy & Astrophysics, 603, A107

Auclair-Desrotour, P. & Leconte, J. 2018, Astronomy & Astrophysics, 613, A45

Auclair-Desrotour, P., Leconte, J., & Mergny, C. 2019, Astronomy & Astrophysics, 624, A17

Bartlett, B. C. & Stevenson, D. J. 2016, Geophysical Research Letters, 43, 5716

Bretherton, F. P. 1969, Quarterly Journal of the Royal Meteorological Society, 95, 754

Chapman, S. & Lindzen, R. S. 1970, Atmospheric tides: thermal and gravitational, Vol. 15 (Springer Science & Business Media)

Correia, A. & Laskar, J. 2001, Nature, 411, 767

Correia, A. C. & Laskar, J. 2003, Icarus, 163, 24

Correia, A. C. & Laskar, J. 2010, Exoplanets, 239

Correia, A. C., Laskar, J., & de Surgy, O. N. 2003, Icarus, 163, 1

Cunha, D., Correia, A. C., & Laskar, J. 2015, International Journal of Astrobiology, 14, 233

Dai, A. & Wang, J. 1999, Journal of the atmospheric sciences, 56, 3874

Deitrick, R. & Goldblatt, C. 2024, Nature Geoscience, 17, 675

Farhat, M., Auclair-Desrotour, P., Boué, G., Deitrick, R., & Laskar, J. 2024, A&A, 684, A49

Farhat, M., Auclair-Desrotour, P., Boué, G., & Laskar, J. 2022, Astronomy & Astrophysics, 665, L1

Gold, T. & Soter, S. 1969, Icarus, 11, 356

Gu, P.-G., Peng, D.-K., & Yen, C.-C. 2019, The Astrophysical Journal, 887, 228

Ingersoll, A. P. & Dobrovolskis, A. R. 1978, Nature, 275, 37

Kelvin, L. o. k. a. W. T. 1882, Proceedings of the Royal Society of Edinburgh, 11, 396

Lamb, H. 1911, Proceedings of the Royal Society of London. Series A, Containing Papers of a Mathematical and Physical Character, 84, 551

Lambeck, K. 1977, Philosophical Transactions of the Royal Society of London Series A, 287, 545

Laskar, J. & Correia, A. C. 2004, in Extrasolar Planets: Today and Tomorrow, Vol. 321, 401

Laskar, J., Farhat, M., Lantink, M. L., et al. 2024, Sedimentologika, 2, 1271

Leconte, J., Wu, H., Menou, K., & Murray, N. 2015, Science, 347, 632

Lee, U. 2020, Monthly Notices of the Royal Astronomical Society, 494, 3141

Lindzen, R. S. & Blake, D. 1972, Journal of Geophysical Research, 77, 2166

Lindzen, R. S. & McKenzie, D. J. 1967, pure and applied geophysics, 66, 90

Mitchell, R. N. & Kirscher, U. 2023, Nature Geoscience, 1

Salazar, A. M. & Wordsworth, R. 2024, The Planetary Science Journal, 5, 218

Schindelegger, M. & Ray, R. D. 2014, Monthly Weather Review, 142, 4872

Wang, H., Boyd, J. P., & Akmaev, R. A. 2016, Geoscientific Model Development, 9, 1477

Wu, H., Murray, N., Menou, K., Lee, C., & Leconte, J. 2023, Science Advances, 9, eadd2499

Zahnle, K. & Walker, J. C. 1987, Precambrian Research, 37, 95